Silicon (2024) 16:3395–3404
https://doi.org/10.1007/s12633-024-02934-9

RESEARCH

Numerical Investigation of Argon Gas Flow Patterns and Their Effects on Mc-Si Ingot Growth Process: Solar Cell Applications

Sugunraj Sekar[1,2] · Srinivasan Manikkam[1,2] · Ramasamy Perumalsamy[1]

Received: 27 December 2023 / Accepted: 25 February 2024 / Published online: 4 March 2024

Abstract
Using the finite volume method, a directional solidification (DS) furnace used to grow a multi-crystalline silicon (mc-Si) ingot is numerically simulated in 2-dimensions. The impact of argon gas flow pattern on the melt-free surface (M-FS) was studied using transient global simulations of oxygen and carbon-dependent transport in laboratory-scale DS furnaces for solar cell applications. Argon gas flow (AGF) patterns over the M-FS affects the temperature of the upper part of the silicon melt. In the conventional furnace, AGF pattern is opposite to the growth direction. In a modified furnace system, argon gas is distributed through the melt vertical to the growth direction. In the modified furnace, during the crystallisation process, the evaporated SiO flux at the top of the M-FS reduces, resulting in a decrease in oxygen concentration in the grown ingot. A modified AGF pattern that inhibits the reaction between SiO gas and hot graphite material shows an exponential reduction of carbon concentration in the as-grown ingot. The conventional ingot obtained the oxygen and carbon concentrations within 6.61E17 and 9.04E16 atoms/cm^3 respectively and the modified ingot obtained the oxygen and carbon impurity concentrations within 2.2E17 and 5.32E16 atoms/cm^3, respectively. The modified AGF pattern improves the quality of mc-Si ingots for PV applications.

Keywords Numerical Simulation · Solar cell · Silicon growth · Impurity · Directional Solidification

1 Introduction

Solar energy is a fundamentally affordable and clean form of energy for the future. It has a number of benefits, including ease of accessibility, scalability, and technological maturity to fulfil the rapidly increasing worldwide need for power and energy. Crystalline Silicon solar cells are primarily responsible for the development of the photovoltaic industry [1–3]. One of the most crucial technologies for the development of multi-crystalline (mc-Si) ingot for photovoltaic applications is the directional solidification (DS) method. Understanding transport processes together with the chemistry of the melt and gas is essential for growing high-quality bulk crystals, i.e. crystals with appropriate defect density and adequate dopant uniformity. Due to the high temperature of the environment, direct experimental examination and in-situ species transport observation are rather challenging. So, crystal growth modeling attracts more attention to improve technology and find an effective way to control mass transport during crystal growth [4]. For solar cells, the mc-Si ingot is a crucial substrate material. The magnitudes of oxygen (O) and carbon (C) in the material have a significant impact on how effectively the processed cells function. Such impurities result in defects, precipitates, and dislocations that serve as photo carrier recombination hubs and lower the conversion efficiency of solar cells. Due to the usage of graphite and O-containing components, C and O, as well as the related gaseous CO and SiO species, are always present in the growing system. During the growth process, the furnace interior materials affect the quality of the mc-Si ingot. The influence of atmospheric CO concentrations and furnace products on mc-Si was investigated, with the concentration of interactions between C- and O-containing species. Rabe et al., experimentally studied the impurity distribution on the mc-Si ingot with and without carbon sources and the coating of the silica crucible. The O concentration in the

✉ Srinivasan Manikkam
srinisastri@gmail.com

[1] Research Centre, Sri Sivasubramaniya Nadar College of Engineering, Chennai 603110, India

[2] Department of Physics, Sri Sivasubramaniya Nadar College of Engineering, Chennai 603110, India

as-grown mc-Si ingot was reduced with an increase in the Si_3N_4 coating thickness of the silica crucible [5]. During the growth, melt convection [6], growth rate [4], argon gas flow (AGF) rates and the furnace pressure affect the impurity transport. Interstitial oxygen is thought to not significantly affect minority carrier lifetime and even increases silicon wafer strength; however, at high concentrations, it promotes the formation of oxygen precipitates that would aid in the nucleation of dislocations during solidification, affecting the electrical properties and conversion efficiency of solar cells. On the other hand, because they serve as the electrical recombination hubs for photocarriers, boron-oxygen (B-O), and silicon-oxygen (Si–O) complexes degrade solar cells [7, 8]. SiO reaction on graphite materials was minimized by installing a molybdenum gas shield on the melt-free surface (M-FS) [9]. The DS technique allows for easy adjustment of the argon flow parameters, including flow rate and furnace pressure, which has an adjustable impact on the convection of the silicon melt. In order to manage and enhance the quality of the solidified mc-Si ingot, it is required to properly define the interactions between the AGF and the melt convection, particularly the effect of the AGF on the melt convection. Reimann et al., demonstrated that, even for a severely polluted feedstock, an mc-Si ingot with an axially and radially uniform impurity concentration could be produced under specific convection conditions [10, 11]. The DS technique allows for easy adjustment of the argon flow parameters, including flow rate and furnace pressure, which has an adjustable impact on the convection of the silicon melt. In order to regulate and enhance the quality of the ingot, it is required to properly define the relations between the AGF and the melt convection, particularly the effect of the argon flow on the melt convection [10]. According to Teng et al., gas guidance system [GGS] can lower the concentration of SiO and CO while increasing gas velocity above M-FS [12]. Bellmann et al., reported that an adaptable tool was used to enhance the characteristics of the mc-Si ingot. The argon injector is to control the AGF patterns in vertical and horizontal directions. Additionally, horizontal gas injection reduces contaminants more effectively than vertical gas injection [13]. The concentration of O and C impurities can be rapidly boosted by the argon backflow at the crucible outlet. A 3D gas guidance system (GGS) was used to study the impurity transport in order to suppress the backflow and reduce the kinetic rate of the reaction and was also experimentally evaluated [14].

In this paper, a transient 2-dimensional axisymmetric global model is implemented to analyze the effects of modified AGF patterns by modified AGF tube on the SiO and CO gas concentration on the M-FS and the O and C concentration in the mc-Si ingot. Additionally, the effect of modified AGF on the melting surface is studied.

2 Model Description

One of the crucial methods utilized to grow mc-Si for PV applications is the DS process. The silica crucible, graphite heaters, insulating walls, heat exchanger, coolant, and graphite supporter for the crucible are the primary components of the DS furnace. The silica crucible is filled with silicon feedstock. High temperatures will cause the silica crucible to deform, so the deformation is prevented by tightening the crucible with the graphite material. The silicon feedstock is then melted by heating the crucible to 1500℃ in the furnace. The temperature is then maintained for a predetermined number of hours to guarantee the homogeneity of the melt. Then, after the slit valve has been opened for heat dispersion, the solidification process starts. Inside the furnace, the pressure maintains at 600 mbar. To reduce the contamination of the silicon melt from the atmosphere a defined inert gas flow above the melt surface can be used. Here we are using the AGF and the flow rate is 20 l/min. After the complete smelting the heater power is reduced.

The simulation was performed after the melting process. Figure 1 shows a schematic diagram of a generation one (G-1) DS furnace system with material table. Using the finite volume method, a DS furnace used to grow a mc-Si ingot is numerically simulated in 2-dimensions. A silica crucible is placed in the center of the DS furnace. Argon gas atmosphere was maintained inside the DS furnace. Hence, the transfer of heat from the heater to the silica crucible is by radiation. Conduction and convection processes are followed by melting and crystallization processes.

In conventional furnaces, AGF directly falls on the surface of the melt, affecting the top of the melt temperature. Therefore, AGF enhances the growth speed at the top of the melt. To increase the AGF above the melting surface, the minimum impurity concentration obtained in the ingot is obtained [12, 15–19] and the M-FS enhances the freezing of the silicon melt top. Based on the above situation, we try to solve the problem by modifying the end of the argon gas tube. In the conventional furnace, AGF patteren is opposite to the growth direction. In a modified furnace system, argon gas is distributed through the melt perpendicular to the growth direction.

The figure below (Fig. 2) shows the dimensions of argon gas tube in conventional and modified furnaces. In a typical case, argon gas is injected at a flow rate of 20 l/min of argon gas, which falls directly onto the M-FS. But in the modified furnace system, the argon gas flow is divided into 10, 10 l/min at the outlet. The argon gas does not fall directly on the M-FS, the intensity of the argon gas is distributed throughout the unmelted surface and the SiO and CO gases are easily removed in the modified furnace.

The advantages of the modified argon gas tube are as follows.

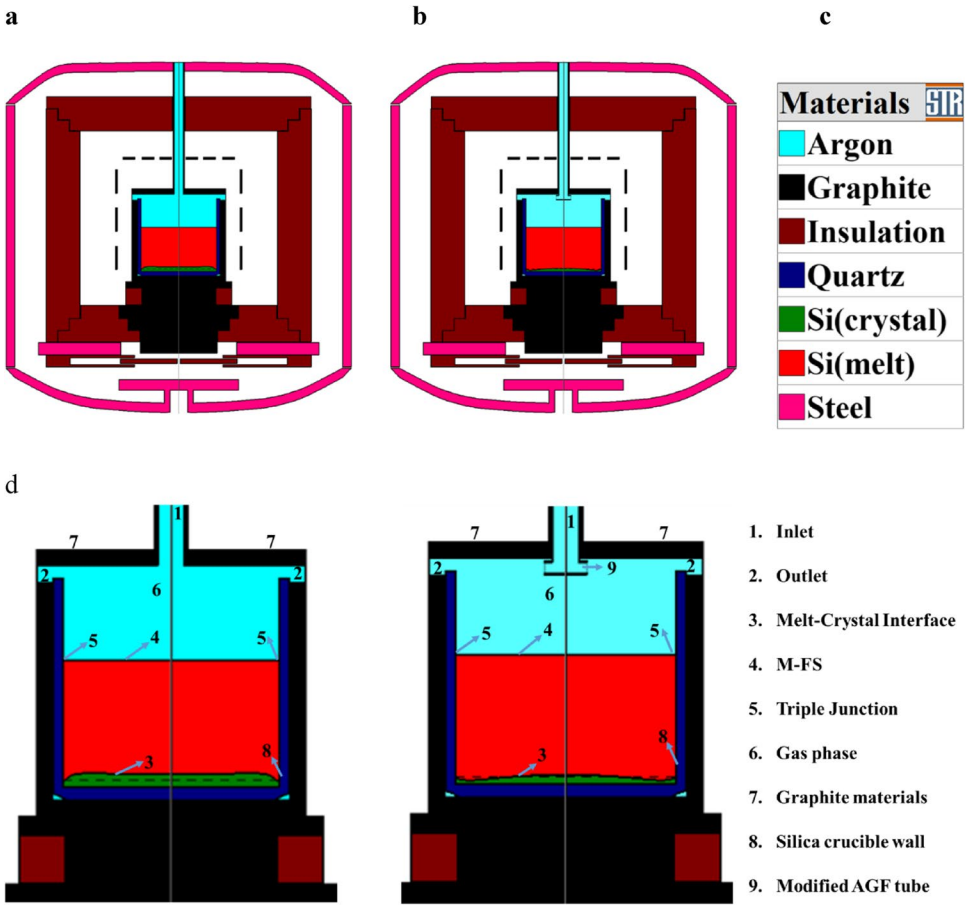

Fig. 1 Schematic diagram of DS furnace. **a** conventional furnace, **b** modified furnace, **c** material table and **d** hot zone of the convrntional and modified furnace

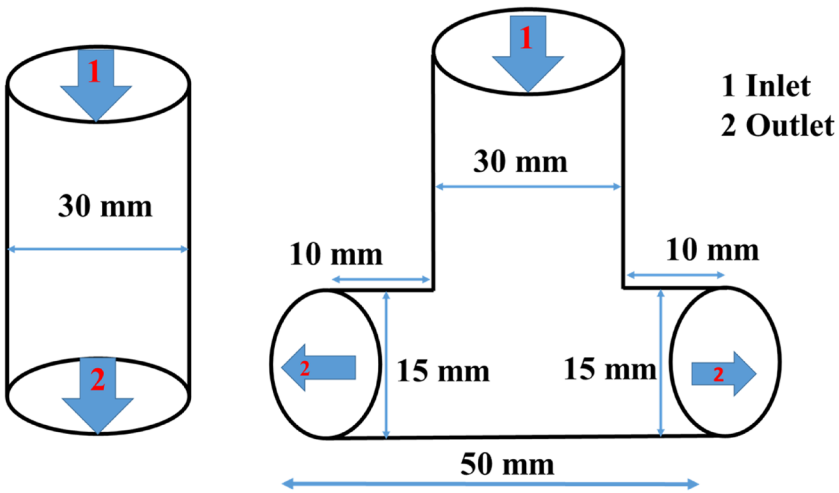

Fig. 2 Left is conventional and right is modified argon gas tube

- Does not affect the temperature above the silicon melt.
- Reduces the reaction of SiO gas with graphite materials.
- Removes CO gas before back diffusion.
- Ingot is obtained with minimum carbon impurity.

The governing equations of mass transport, heat transport and species transport are as follows:

$$\frac{\partial \rho}{\partial t} + \nabla \cdot \left(\rho \vec{u}\right) = 0 \tag{1}$$

$$\frac{\partial \left(\rho C_p T\right)}{\partial t} + \nabla \cdot \left(\rho C_p \vec{u} T\right) = \nabla \cdot \left(\lambda_{eff} \nabla T\right) - \nabla \cdot \overrightarrow{q_{rad}} + S_T \tag{2}$$

$$\frac{\partial(\rho\varphi_i)}{\partial t} + \cdot\left(\rho\vec{u}\varphi_i\right) = \nabla\cdot\left(D_{\varphi_i eff}\varphi_i\right) + S_{\varphi_i} \tag{3}$$

where ρ is density, $\vec{u}$ is velocity, C_p is specific heat, T is temperature, $\lambda_{eff} = \lambda + \frac{C_p\mu_t}{Pr_t}$ is the effective thermal conductivity, Pr_t=0.9 is the turbulent Prandtl number, $\overrightarrow{q_{rad}}(r) = \int_0^\infty \oint_{4\pi} \Omega I_\lambda(r,\Omega)d\Omega\mathrm{d}\lambda$ is the vector radiative heat flux, $I_\lambda(r,\Omega)$ is the intensity of the radiation at the point r, λ is the wavelength of the radiation, $D_{\varphi_i\ eff}$ is the effective dynamic diffusivity, $S_{\varphi_i} = S^u_{\varphi_i} + \phi_i S^P_{\varphi_i}$ stands for the ith species source [20].

The growth velocity at the S-L interface is obtained by the following equation:

$$V_{crys} = \frac{1}{|n_x|\rho_{crys}\Delta H}\left(\lambda_{crys}\frac{\partial T_{crys}}{\partial n} - \lambda_{melt}\frac{\partial T_{melt}}{\partial n} + \left(Q^{in}_{rad} - Q^{out}_{rad}\right)_{crys} - \left(Q^{in}_{rad} - Q^{out}_{rad}\right)_{melt}\right) \tag{4}$$

V_{crys} is crystallization rate, n is normal to the interface surface, n_x is the cosine angle between the normal n and vertical angle, ρ_{crys} is crystal density, ΔH is the latent heat, λ_{crys} and λ_{melt} are thermal conductivities in the crystal and melt respectively, $\frac{\partial T_{crys}}{\partial n}$ and $\frac{\partial T_{melt}}{\partial n}$ are the normal derivatives at the interface in the crystal and melt respectively.

The relative growth velocity and move nodes belonging to the crystallization front is given by Eqs. (5) and (6) respectively.

$$V^{relative}_{crys} = V^{*}_{crys} - V_{crys} \tag{5}$$

$$\Delta X = V^{relative}_{crys} \bullet \Delta t \tag{6}$$

Boundary condition on the crystallization front (the interface) can be written as

$$F_m = (1 - k_{seg})\rho v_{cr} C_{melt} \tag{7}$$

where, ρ, V_{cr} and F_m are the species crystal density, crystallization rate, and, mass flux, respectively. For simulating radiation exchange within transparent or semi-transparent materials, the Discrete Ordinate (DO) model is utilized. This model takes into account a number of boundary constraints, especially at the interfaces between semi-transparent blocks with varying refractive indices or between different types of media.

The governing equation for the oxygen and carbon transport in the silicon feedstock is

$$\frac{\partial(\rho_{si}C_{O)}}{\partial t} + \frac{\partial}{\partial x_i}\left(\rho_{si}u_iC_O\right) = D_{eff}\frac{\partial^2 C_O}{\partial {x_i}^2} \tag{8}$$

$$\frac{\partial(\rho_{si}C_{C)}}{\partial t} + \frac{\partial}{\partial x_i}\left(\rho_{si}u_iC_C\right) = D_{eff}\frac{\partial^2 C_C}{\partial {x_i}^2} \tag{9}$$

Here, C_O and C_C, D_{eff} are the concentration of oxygen, carbon and effective dynamic diffusivity respectively. Below mentioned governing equations give the SiO and CO transport in the argon gas

$$\frac{\partial(\rho_{Ar}\omega_{SiO)}}{\partial t} + \frac{\partial}{\partial x_i}\left(\rho_{Ar}u_i\omega_{SiO}\right) = D_{SiO}\frac{\partial^2(\rho_{Ar}\omega_{SiO)}}{\partial {x_i}^2} \tag{10}$$

$$\frac{\partial(\rho_{Ar}\omega_{CO)}}{\partial t} + \frac{\partial}{\partial x_i}\left(\rho_{Ar}u_i\omega_{CO}\right) = D_{CO}\frac{\partial^2(\rho_{Ar}\omega_{CO)}}{\partial {x_i}^2} \tag{11}$$

Here, ω_{SiO} and ω_{CO} are the mass fraction of SiO and CO gas in the melt-free surface and D_{CO} and D_{SiO} are the diffusivity of CO and SiO respectively.

The carbon boundary condition on the crucible wall was zero flux. Zero fluxes of SiO and CO were used for non-carbon walls and the symmetry axis in gas; zero concentrations of SiO and CO were used for the gas input; and zero gradients of SiO and CO were used for the gas exit [21, 22].

3 Chemical Model

The melt transports the dissolved O from the silicon nitride layer and silica crucible to the melt-crystal interface, where it either becomes a part of the solid or evaporates as SiO from the M-FS. The SiO is transported to the heated graphite fixtures by argon gas, where it combines with carbon to produce CO. CO diffuses into the melt at the M-FS, and then C and O are eventually absorbed into the solid. In solar cells, O-related flaws shorten the lifetime of the minority carrier. C precipitates can lead to wire-sawing flaws, the creation of locally induced tensions, the nucleation of new grains, and ohmic shunts in solar cells. The below mentioned equations explain the chemical reactions that occur inside the DS furnace [22–24].

$$Si_3N_4\ (Solid) = 3Si\ (melt) + 4N\ (melt) \tag{12}$$

$$Si\ (melt) + SiO_2\ (solid) = 2SiO\ (gas) \tag{13}$$

$$SiO_2\ (sold) = Si\ (melt) + 2O\ (melt) \quad (14)$$

$$Si\ (melt) + O\ (melt) = SiO\ (gas) \quad (15)$$

$$SiO\ (gas) + C\ (solid) = CO\ (gas) + Si\ (gas) \quad (16)$$

$$C\ (solid) + SiO_2(solid) = SiO\ (gas) + CO\ (gas) \quad (17)$$

$$CO\ (gas) + 2Si\ (gas) \leftrightarrow\ SiC\ (solid) + SiO\ (gas) \quad (18)$$

$$Si\ (gas) = Si\ (melt) \quad (19)$$

$$CO\ (gas) = C\ (melt) + O\ (melt) \quad (20)$$

$$C\ (melt) = C\ (crystal) \quad (21)$$

$$O\ (melt) = O\ (crystal) \quad (22)$$

4 Result and Discussion

4.1 Effect of AGF on the Melt Surface

The influence of AGF on the transport of O and C in the furnace is studied. The AGF rate was maintained at 20 l/min with a furnace pressure 600 mbar. The argon gas injected on the M-FS is analyzed in different ways (i,e) one is opposite to the growth direction which is the conventional furnace system and another one is perpendicular to the growth direction is the modified furnace system.

The SiO gas distributions on the M-FS are different for different AGF densities on the melt surface as shown in Fig. 3. In the conventional system, the SiO gas distribution on the gas phase is more than on the M-FS. However, a low SiO gas concentration was obtained due to the densities of AGF pattern in the middle of the M-FS. Therefore, more SiO gas is pushed towards the sidewall from the higher to lower AGF density regions. The concentration of the SiO

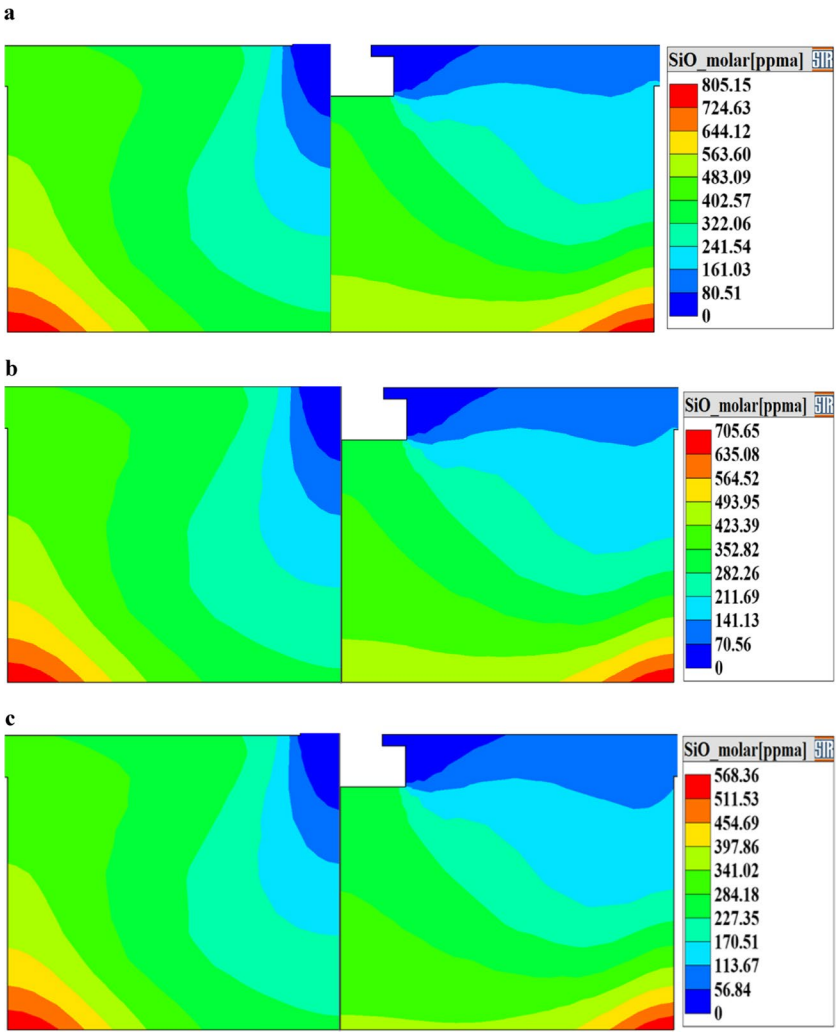

Fig. 3 SiO gas concentration in the M-FS. Left is conventional and right is modified furnace. **a**, **b** and **c** are the 25, 50 and 75% solidified ingot

gas varies from 805.15 to 568.36 ppma. The maximum value of SiO gas concentration is obtained at the triple junction (Silica crucible, Silicon melt and gas phase) of the system. The O- atoms enter the silicon melt from the silica crucible, and react with silicon melt to form SiO gas, which moves towards the M-FS. Due to the heterogeneous argon gas density on the M-FS, the maximum SiO gas concentration was obtained at the triple junction of the furnace. in the conventional furnace, AGF is not sufficient to reduce the SiO gas concentration at the top of the silicon melt.

In the modified furnace system, the minimum SiO gas concentration was obtained due to the higher AGF density at the top of the M-FS. A large concentration of SiO gas is carried away from the M-FS by the modified AGF pattern. The minimum SiO gas concentrations are shown in Fig. 3. At the top of the M-FS, the SiO gas concentration is obtained below 161.03 ppma. However, the bottom of the M-FS received the maximum SiO gas concentration, which enhances the back diffusion of SiO gas and increases oxygen precipitation from the ingot. In the modified furnace system, AGF slightly affects the concentration of SiO gas at the bottom of the M-FS. The advantage of the modified gas flow is reduced reaction between the hot graphite parts and the SiO gas. During the growth process, the modified furnace system reduces the chemical reaction.

The CO gas distribution at the M-FS for different solidification rates is shown in Fig. 4. In a conventional system, the distribution of CO gas on the M-FS is high when SiO gas reacts with the graphite material. However, a lower CO gas concentration was obtained from the graphite-free material region on the M-FS. Therefore, more CO gas is formed near the graphite material. Then, the CO gas gets into the melt after the process of convection and back diffusion. AGF is opposite to the growth direction and is insufficient to reduce CO gas formation. Extraction of SiO gas from the M-FS plays an important role in

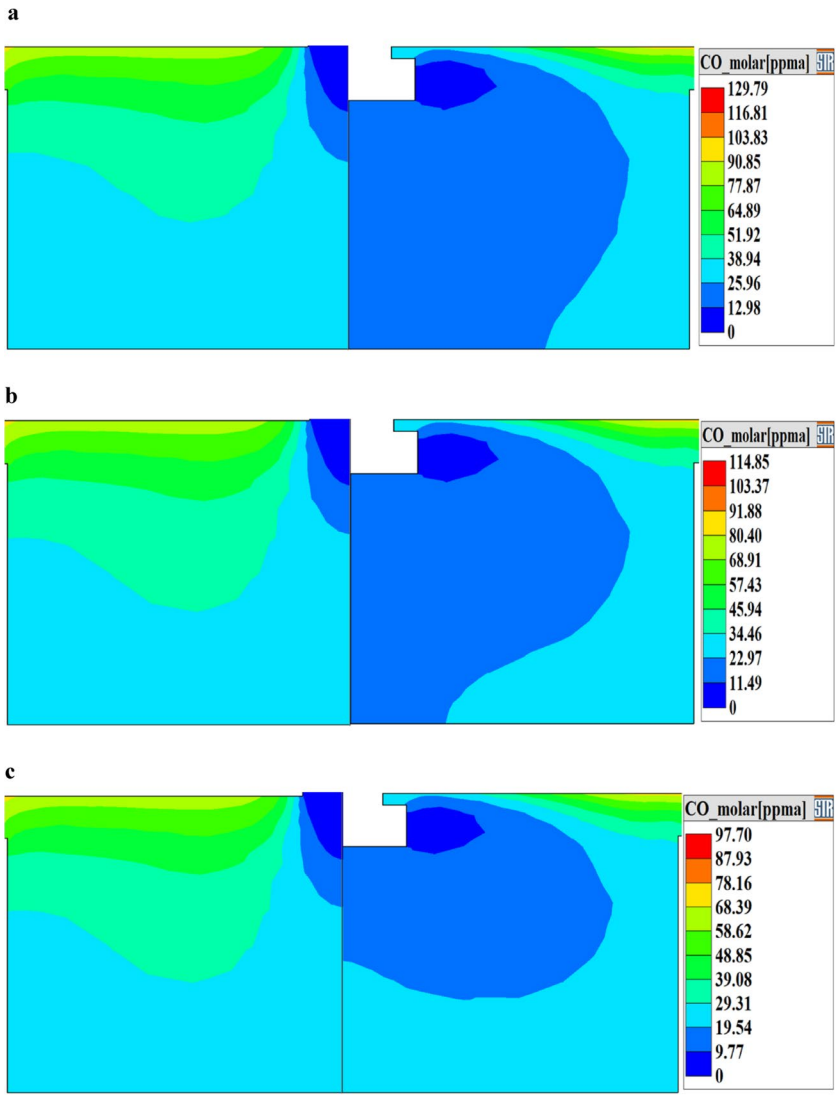

Fig. 4 CO gas concentration in the M-FS. Left is conventional and right is modified furnace. **a**, **b** and **c** are the 25, 50 and 75% solidified ingot

the concentration of CO gas. The obtained CO gas concentration varied from 129 to 9.77 ppma. Increasing the CO gas concentration on the M-FS increases the O and C concentration in the as-grown mc-Si ingot and also affects the quality [25].

In the modified furnace system, the minimum CO gas concentration was obtained due to the high AGF density at the top of the M-FS near the graphite material. Modified AGF reduced high levels of CO gas formation on the M-FS. As shown in Fig. 4 the modified furnace system obtained minimum CO gas concentration. At the M-FS, the CO gas concentration is obtained below 90 ppma. CO gas formation was reduced by more SiO gas carried from the modified furnace. In this case, the back diffusion of CO gas is reduced. So, the minimum CO gas concentration is obtained in the middle of the M-FS.

4.2 Impurity Analysis

4.2.1 O Concentration

A major impurity in the mc-Si ingot is O due to the use of silica crucible. During growth, O is dissolved from the silica crucible. From the solar cell applications, the O concentration less than 1.5E17 atoms/cm^3 is not sufficient to enhance the LID effect [24, 25]. Figure 5 shows the O concentration in a mc-Si ingot grown using the 100% melt. Since the segregation coefficient of oxygen is 1.25, the oxygen concentration increases from the top to the bottom of the ingot. However, the corner of the grown ingot receives a higher oxygen concentration. Due to the segregation of impurities into the melt during solidification, the top of the ingot is particularly affected, as are the margins, which come into direct contact with the crucible walls. In conventional ingot, SiO and CO gases are pushed towards the side wall, so maximum O concentration is achieved by back diffusion of SiO and CO gases in the wall region. O concentration varies from 2.00E15 to 1.10E18 atoms/cm^3. This kind of grown mc-Si ingots can easily induce LID effects for solar cell applications [26, 27]. SiO and CO gas concentrations affect O precipitation in the as-grown mc-Si ingot. Therefore, conventional AGF does not reduce O precipitation in the ingot.

The O concentration of the modified furnace varied from 2.00E15 to 8.80E17 atoms/cm^3. Compared to the conventional furnace, the modified furnace obtains a lower oxygen concentration, which improves the extraction of SiO and CO gas on the M-FS. The surface area with O-concentration below 2.22E17 atoms/cm^3 increases in the grown ingot. The O concentration near the crucible wall is reduced due to the uniformly distributed SiO and CO gas concentrations in the middle of the M-FS. The modified ingot suppresses the LID effect and SiO_2 cluster formation in the ingot.

4.2.2 C Concentration

The dislocation density and electrical activity of the mc-Si ingot are greatly influenced by the C concentration [28–31]. The efficiency of solar cells is decreased due to the C precipitates in silicon ingots, which also have an impact on the wafer-cutting procedure. Figure 6 shows the C concentration in a mc-Si ingot grown using the 100% melt. Typically, the graphite material inside the DS furnace is the main source of the carbon. The C segregation coefficient is 0.07 [29].

The segregation coefficient increases the obtained C concentration from the bottom to the top of the grown ingot. The C concentration in conventional and modified ingots ranged from 1.60E16 to 1.40E17 and 1.60E16 to 1.03E17 atoms/cm^3. During growth, the SiC particle precipitation is enhanced in the conventional furnace [29–35]. At large amounts of CO gas dissolves in the molten silicon C contamination increases in the silicon ingot. On the M-FS, the conventional furnace system is insufficient to reduce the reaction of hot graphite materials and SiO gas. The modified furnace prevents the reaction between hot graphite materials and SiO gas. So, the modified ingot obtained the lowest C concentration compared to the conventional ingot due to the change in AGF.

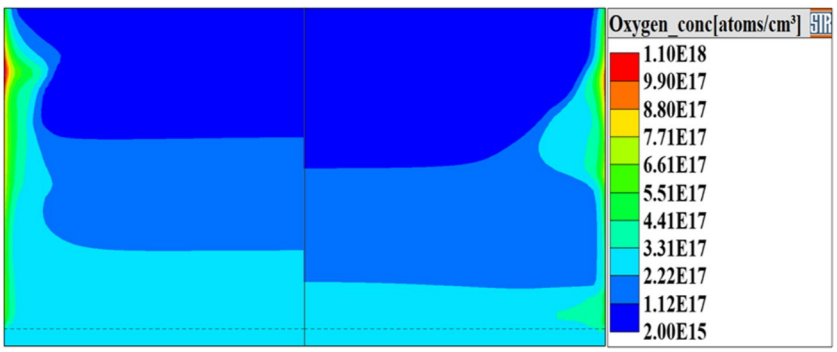

Fig. 5 Shows the O concentration in a mc-Si ingot grown using the 100% melt: left is conventional and right is modified furnace

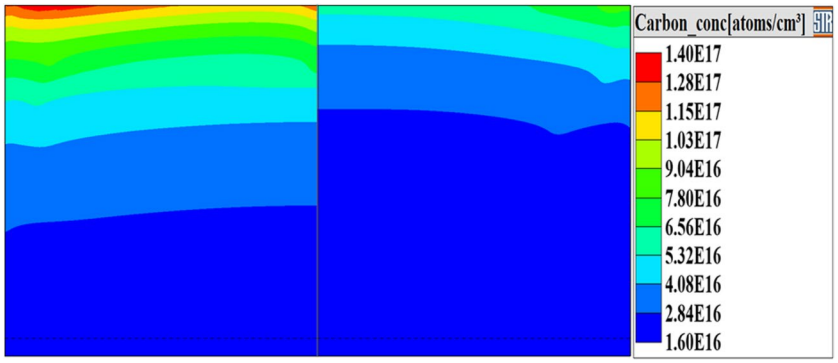

Fig. 6 Shows the C concentration in a mc-Si ingot grown using the 100% melt: left is conventional and right is modified furnace

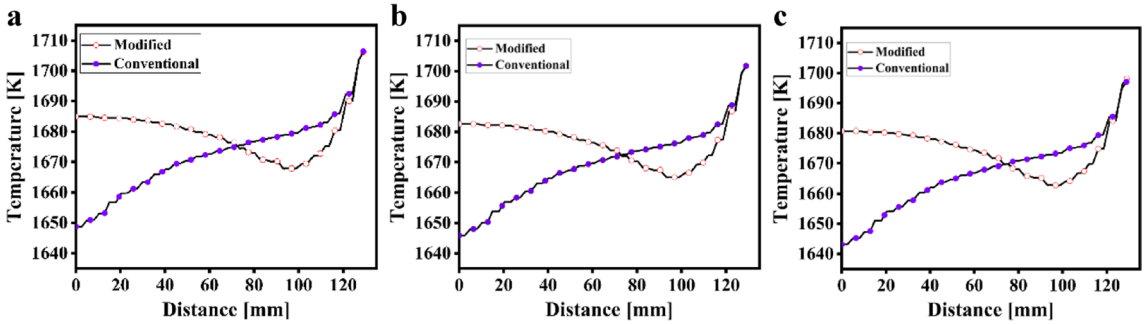

Fig. 7 Temperature distribution on the M-FS. **a**, **b** and **c** are after the 25, 50 and 75% solidification

4.3 Temperature Analysis on the M-FS

Figure 7 shows the temperature distribution on the top of the M-FS. The temperature distribution data are noted at the 50 mm top of the M-FS for both cases. The AGF on the M-FS affects the temperature of the top silicon melt. The conventional AGF flow directly falls on top of the silicon melt, enhancing the multi-nucleation at the top of the grown ingot. The melt flow pattern and vortex formation enhance the AGF on the M-FS. The modified furnace AGF pattern does not directly fall on the top of the melt and it reaches the top of the melt is 10 l/min which is shown in Fig. 2. The temperature distribution affects the modified furnace less compared to the conventional furnace. During the growth process, increase in the AGF reduces the impurity concentration in the grown mc-Si ingot. But, in the conventional ingot increase in the AGF above 30 l/min on the melt surface tends to freeze [21]. In the modified furnace system AGF upto 60 l/min can be used.

5 Conclusion

We carried out numerical simulations of global heat transfer in a DS furnace for the mc-Si ingot growth process. O and C concentrations of mc-Si ingot in DS furnaces with modified AGF tube is investigated. During the growth process, the modified AGF reduces the back diffusion of CO and transports more SiO gas from the DS furnace. On the other hand, the C concentration decreases largely in the mc-Si ingot due to less CO gas formation. O concentration was obtained due to reduced back diffusion of SiO gas in the modified ingot. In the conventionally grown ingot the obtained oxygen and carbon concentrations are within 6.61E17 and 9.04E16 atoms/cm^3 respectively and in the modified furnace the obtained oxygen and carbon impurity concentrations are within 2.2E17 and 5.32E16 atoms/cm^3, respectively. In the conventional furnace, the AGF pattern affects the temperature of the silicon melt surface. In the moidified furnace, the effect of temperature in the M-FS is low compared to the conventional furnace. So, a higher AGF rate is possible in the modified furnace. Based on the above discussion, modified furnace gives a better quality of the mc-Si ingot for PV applications.

Acknowledgements This work is supported by the Department of Science and Technology, Government of India (Order No. DST/TMD/CERI/RES/2020/7 dated on 31/12/2020).

Author Contributions Sugunraj Sekar—wrote the main manuscript.
Srinivasan Manikkam—reviewed the manuscript.
Ramasamy Perumalsamy—reviewed the manuscript.

Funding Not Applicable.

Data Availability No datasets were generated or analysed during the current study.

Code Availability Not Applicable.

Declarations

Compliance with Ethical Standards This study involving human participants were in accordance with the ethical standards of the institutional and/or national research committee.

Consent to Participate Informed consent was obtained from all individual participants included in the study.

Consent for Publication Consent for publication was obtained from all individual participants included in the study.

Competing Interests The authors declare no competing interests.

References

1. Popovich VA, Geerstma W, Janssen M et al (2015) Mechanical strength of silicon solar wafers characterized by ring-on-ring test in combination with digital image correlation. In: TMS Annual Meeting. John Wiley & Sons, Inc., Hoboken, NJ, USA, p 241–248
2. Blakers A, Zin N, McIntosh KR, Fong K (2013) High efficiency silicon solar cells. Energy Procedia 33:1–10. https://doi.org/10.1016/j.egypro.2013.05.033
3. Matsuo H, Bairava Ganesh R, Nakano S et al (2008) Thermodynamical analysis of oxygen incorporation from a quartz crucible during solidification of multicrystalline silicon for solar cell. J Cryst Growth 310:4666–4671. https://doi.org/10.1016/j.jcrysgro.2008.08.045
4. Trempa M, Reimann C, Friedrich J, Müller G (2010) The influence of growth rate on the formation and avoidance of C and N related precipitates during directional solidification of multi crystalline silicon. J Cryst Growth 312:1517–1524. https://doi.org/10.1016/j.jcrysgro.2010.02.005
5. Raabe L, Pätzold O, Kupka I et al (2011) The effect of graphite components and crucible coating on the behaviour of carbon and oxygen in multicrystalline silicon. J Cryst Growth 318:234–238. https://doi.org/10.1016/j.jcrysgro.2010.11.142
6. Gao B, Nakano S, Kakimoto K (2013) Reduction of oxygen impurity in multicrystalline silicon production. Int J Photoenergy 2013:1–6. https://doi.org/10.1155/2013/908786
7. Modanese C, Di Sabatino M, Søiland AK et al (2011) Investigation of bulk and solar cell properties of ingots cast from compensated solar grade silicon. Prog Photovoltaics Res Appl 19:45–53. https://doi.org/10.1002/pip.986
8. Kerkar F, Kheloufi A, Dokhan N et al (2020) Oxygen and Carbon Distribution in 80Kg Multicrystalline Silicon Ingot. SILICON 12:473–478. https://doi.org/10.1007/s12633-019-00154-0
9. Kumar MA, Srinivasan M, Ramasamy P (2021) Reduction of Carbon and Oxygen Impurities in mc-Silicon Ingot Using Molybdenum Gas Shield in Directional Solidification Process. SILICON 13:4535–4544. https://doi.org/10.1007/s12633-020-00775-w
10. Li Z, Liu L, Liu X et al (2012) Effects of argon flow on melt convection and interface shape in a directional solidification process for an industrial-size solar silicon ingot. J Cryst Growth 360:87–91. https://doi.org/10.1016/j.jcrysgro.2011.11.053
11. Reimann C, Trempa M, Friedrich J, Müller G (2010) About the formation and avoidance of C and N related precipitates during directional solidification of multi-crystalline silicon from contaminated feedstock. J Cryst Growth 312:1510–1516. https://doi.org/10.1016/j.jcrysgro.2010.02.003
12. Teng YY, Chen JC, Huang BS, Chang CH (2014) Numerical simulation of impurity transport under the effect of a gas flow guidance device during the growth of multicrystalline silicon ingots by the directional solidification process. J Cryst Growth 385:1–8. https://doi.org/10.1016/j.jcrysgro.2013.01.040
13. Bellmann MP, Lindholm D, M'Hamdi M (2014) A novel method for gas flow and impurity control in directional solidification of multi-crystalline silicon. J Cryst Growth 399:33–38. https://doi.org/10.1016/j.jcrysgro.2014.04.019
14. Su W, Li J, Li C et al (2022) Design and Numerical Optimization of Gas Guidance System in Casting Silicon Furnace by the Orthogonal Experiment. SILICON 14:301–307. https://doi.org/10.1007/s12633-021-01192-3
15. Mukaiyama Y, Fukui Y, Taishi T, Artemiev V, Noda Y, Sueoka K (2022) Numerical Modeling and Evaluation of Constitutional Supercooling during Silicon Single Crystal Growth by Cz Method. In: The 8th International Symposium on Advanced Science and Technology of Silicon Materials
16. Kalaev VV (2012) Liquid flow in a cubic cavity generated by gas motion along the free surface. Int J Heat Mass Transf 55(19–20):5214–5221
17. Nguyen THT, Liao SH, Chen JC, Chen CH, Huang YH, Yang CJ, ..., Nguyen HB (2016) Effects of the hot zone design during the growth of large size multi-crystalline silicon ingots by the seeded directional solidification process. J Cryst Growth 452:27–34.
18. Liu X, Dang Y, Tanaka H, Fukuda Y, Kutsukake K, Kojima T, ..., Usami N (2022) Data-driven optimization and experimental validation for the lab-scale mono-like silicon ingot growth by directional solidification. ACS Omega 7(8):6665–6673
19. Sugunraj S, Aravindan G, Srinivasan M, Ramasamy P (2023) Influence of Argon Gas Flow Rate on Oxygen and Carbon Impurities Concentration in Multicrystalline Silicon Grown by Directional Solidification Furnace: Numerical and Experimental Investigation. SILICON 15:1701–1724. https://doi.org/10.1007/s12633-022-02097-5
20. Liu X, Gao B, Kakimoto K (2015) Numerical investigation of carbon contamination during the melting process of Czochralski silicon crystal growth. J Cryst Growth 417:58–64
21. Häßler C, Hofs HU, Koch W et al (2000) Formation and annihilation of oxygen donors in multicrystalline silicon for solar cells. Mater Sci Eng B Solid-State Mater Adv Technol 71:39–46. https://doi.org/10.1016/S0921-5107(99)00346-3
22. Lan CW, Hsu C, Nakajima K (2015) Multicrystalline Silicon Crystal Growth for Photovoltaic Applications. In: Handbook of crystal growth: bulk crystal growth. Elsevier, pp 373–411. https://doi.org/10.1016/B978-0-444-63303-3.00010-9
23. Giannattasio A, Senkader S, Azam S et al (2003) The use of numerical simulation to predict the unlocking stress of dislocations in Cz-silicon wafers. Microelectron Eng 70:125–130. https://doi.org/10.1016/S0167-9317(03)00434-9
24. Saitoh T, Hashigami H, Rein S, Glunz S (2000) Overview of light degradation research on crystalline silicon solar cells. Prog Photovolt Res Appl 8(5):537–547. https://doi.org/10.1002/1099-159X(200009/10)8:5%3C537::AID-PIP349%3E3.0.CO;2-W
25. Sekar S, Thamodharan K, Manikkam S, Nallusamy N, Perumalsamy R (2023) Numerical investigation of the effect of modified heat exchanger block on thermal stress and dislocation density of DS-Grown mc-Si Ingot. Cryst Res Technol 2200285. https://doi.org/10.1002/crat.202200285
26. Qi X, Liu L, Ma W (2017) Effects of furnace pressure on oxygen and carbon coupled transport in an industrial directional solidification furnace for crystalline silicon ingots. J Cryst Growth 468:933–938. https://doi.org/10.1016/j.jcrysgro.2016.10.027

27. Lindroos J, Savin H (2016) Review of light-induced degradation in crystalline silicon solar cells. Sol Energy Mater Sol Cells 147:115–126. https://doi.org/10.1016/j.solmat.2015.11.047
28. Pizzini S, Sandrinelli A, Beghi M et al (1988) Influence of Extended Defects and Native Impurities on the Electrical Properties of Directionally Solidified Polycrystalline Silicon. J Electrochem Soc 135:155–165. https://doi.org/10.1149/1.2095543
29. Bornside DE, Brown RA, Fujiwara T et al (1995) The Effects of Gas-Phase Convection on Carbon Contamination of Czochralski-Grown Silicon. J Electrochem Soc 142:2790–2804. https://doi.org/10.1149/1.2050094
30. Liu L, Nakano S, Kakimoto K (2008) Carbon concentration and particle precipitation during directional solidification of multicrystalline silicon for solar cells. J Cryst Growth 310:2192–2197. https://doi.org/10.1016/j.jcrysgro.2007.11.165
31. Sekar S, Gurusamy A, Manikkam S et al (2023) Improvement of DS Grown Mc-Si Ingot for PV Application by Reducing the Thickness of the Bottom Heat Exchanger Block: Numerical Investigation. SILICON 15:4183–4192. https://doi.org/10.1007/s12633-023-02350-5
32 Sekar S, Thamotharan K, Manickam S, Murugesan B, Kakimoto K, Perumalsamy R (2024) A critical review of the process and challenges of silicon crystal growth for photovoltaic applications. Cryst Res Technol 59(1):2300131
33. Kesavan V, Srinivasan M, Ramasamy P (2019) The Influence of Multiple-Heaters on the Reduction of Impurities in mc-Si for Directional Solidification. SILICON 11:1335–1344. https://doi.org/10.1007/s12633-018-9928-7
34. Bharathwaj M, Sugunraj S, Karuppasamy P et al (2023) Effect of argon flow rate on mc-Silicon Ingot Grown by DS process for PV application: a numerical investigation of non-metallic impurities. Silicon 15:5937–5946. https://doi.org/10.1007/s12633-023-02490-8
35. Sekar S, Manikkam S, Perumalsamy R (2023) Investigation of Solid-Liquid interface effects on the impurity concentration in the DS grown Mc-Si Ingot by using C-Clamp insulation block for solar cell applications: numerical analysis. SILICON. https://doi.org/10.1007/s12633-023-02839-z